Title

A critical signal for phenotype transition driven by negative feedback loops.

Journal

iScience, 27(1)

Authors

Wang, Yao
Dong, Yingying
Zhai, Qiaocheng
et al.

Publication Date

2024-01-19

DOI

10.1016/j.isci.2023.108716

Peer reviewed

iScience

CellPress
OPEN ACCESS

Article

A critical signal for phenotype transition driven by negative feedback loops

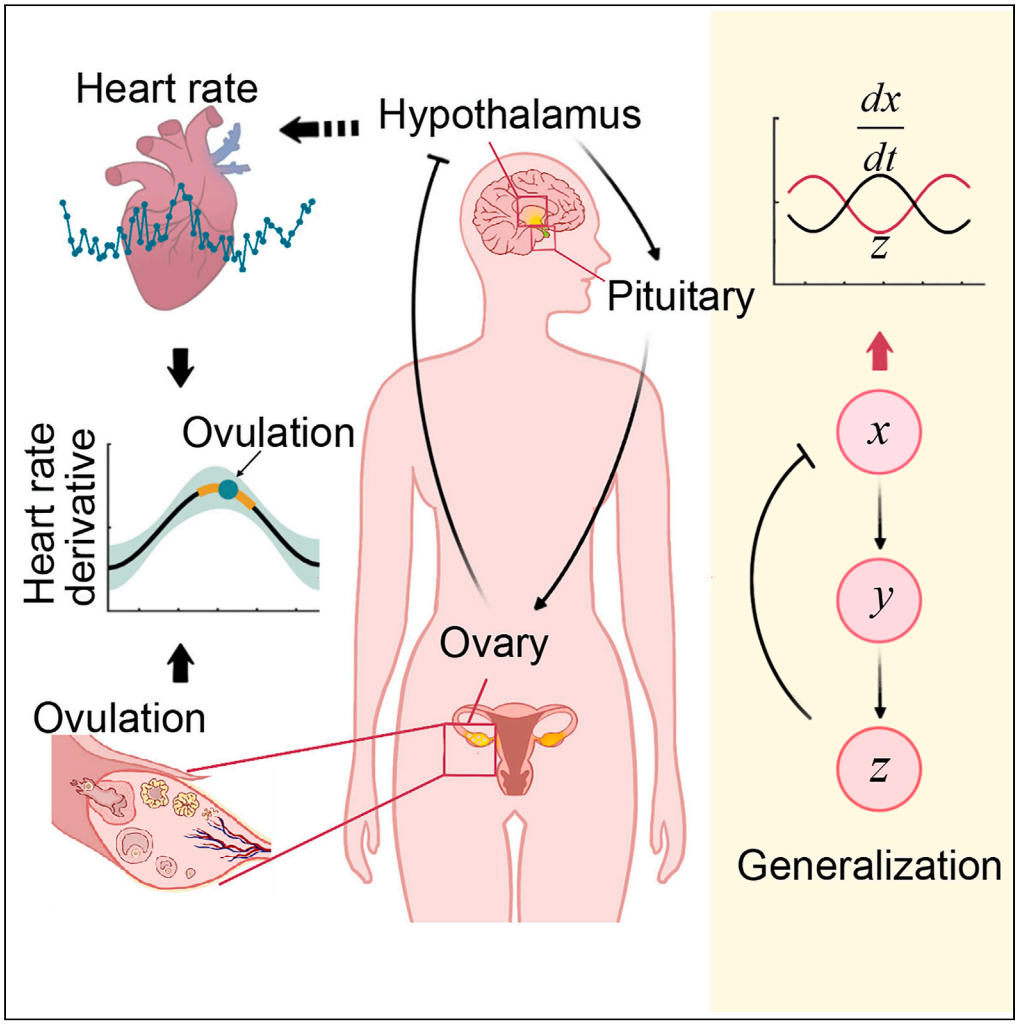

Yao Wang, Yingying Dong, Qiaocheng Zhai, Wei Zhang, Ying Xu, Ling Yang

yingxu@suda.edu.cn (Y.X.)
lyang@suda.edu.cn (L.Y.)

Highlights

Ovulation corresponds to the maximum of the daily average heart rate derivative

Offset of mice activity corresponds to the derivative maxima of calcium signal

A general model for revealing derivative maxima as biomarkers of activity is built

Wang et al., iScience 27, 108716
January 19, 2024
https://doi.org/10.1016/j.isci.2023.108716

iScience

CellPress
OPEN ACCESS

Article

A critical signal for phenotype transition driven by negative feedback loops

Yao Wang,[1,2,5] Yingying Dong,[3,5] Qiaocheng Zhai,[3] Wei Zhang,[4] Ying Xu,[3,*] and Ling Yang[1,2,6,*]

SUMMARY

The biological rhythms governed by negative feedback loops have undergone extensive investigation. However, developing reliable and versatile warning signals to predict periodic fluctuations in physiological processes and behaviors associated with these rhythms remains a challenge. Here, we monitored the heart rate and tracked ovulation dates of 91 fertile women. The finding strongly links the velocity (derivative) of heart rate with ovulation in menstrual cycles, providing a predictive warning signal. Similarly, an analysis of calcium signaling in the suprachiasmatic nucleus (SCN) of mice reveals that the maximum velocity of rising calcium signal aligns with locomotor activity offsets. To demonstrate the generality of derivative-transitions link, numerical simulations using a negative feedback loop model were conducted. Statistical analysis indicated that over 90% of the oscillations exhibited a correlation between maximum velocity and transition points. Consequently, the maximum velocity derived from oscillatory curves holds significant potential as an early warning signal for critical transitions.

INTRODUCTION

Oscillatory phenomena are prevalent in biological systems and are often driven by time-delayed negative feedback loops, including circadian rhythms,[1] monthly cycles,[2] and seasonal cycles.[3] Negative feedback loops are critical for the cyclical physiological and behavioral transitions, such as activity-rest, ovulation, and blood pressure regulation. However, accurately predicting or capturing tipping points in oscillations before a critical transition occurs remains a notable challenge in the field.

The female menstrual cycle is a complex monthly process that involves menstruation, the follicular phase, ovulation, and the luteal phase. This cycle is governed by the hypothalamic-pituitary-ovarian axis through multiple feedback loops.[4–8] Each phase is strictly controlled by hormones produced by the hypothalamus, pituitary gland, and ovaries.[9] Previous studies have suggested using heart rate variability,[10] blood pressure,[11] and body temperature[12] as early warning signals for menstrual cycle phase transitions. Machine learning algorithms have also been developed to predict ovulation by integrating various physiological parameters, including heart rate.[13] However, these indicators lack universality and detailed mechanistic understanding.

Heart rates are regulated by the autonomic nervous system in order to maintain homeostatic balance: the parasympathetic nervous system decreases heart rate, while the sympathetic nervous system increases heart rate.[14] The heart rate pattern is shaped by humoral and neural feedbacks, as well as circadian commands. Given that heart rate and heart rate oscillations both depend on balanced activation and inhibition, we aim at disentangling true heart rate oscillations driven by the menstrual cycle that link to the ovulation phase. Negative feedback loops are generated through activator-induced inhibitor regulatory motifs with assigned functions for input-output behavior.[15] The mechanism of this inhibitory function involves modifying the rate of change of the suppressed factor, which can be realized by accelerating the degradation or promoting the production of the inhibited factor. Therefore, it is plausible that estimating velocity trajectories based on oscillation curves allows for inferences in predicting tipping points.

Here, we enrolled fertile women and used menopausal women and men as negative controls. We recorded their heartbeats using wearable devices, as previously described.[16] We focused on identifying patterns related to ovulation and determining whether velocity trajectories could help identify critical points or early warning signals for ovulation. We also examined whether these velocity trajectories could be applied to other oscillatory phenomena, such as calcium signals in the suprachiasmatic nucleus (SCN) that facilitate forward locomotion. Finally, we used a three-variable negative feedback oscillator model to analyze the relationship between velocity trajectories and the trough phase of transition points along the oscillatory curve.

[1]School of Mathematical Science, Soochow University, Suzhou 215006, China
[2]Center for Systems Biology, Soochow University, Suzhou 215006, China
[3]Jiangsu Key Laboratory of Neuropsychiatric Diseases and Cambridge-Su Genomic Resource Center, Suzhou medical college of Soochow University, Suzhou 215123, China
[4]Institute of Science and Technology for Brain-Inspired Intelligence, Fudan University, Shanghai 200433, China
[5]These authors contributed equally
[6]Lead contact
*Correspondence: yingxu@suda.edu.cn (Y.X.), lyang@suda.edu.cn (L.Y.)
https://doi.org/10.1016/j.isci.2023.108716

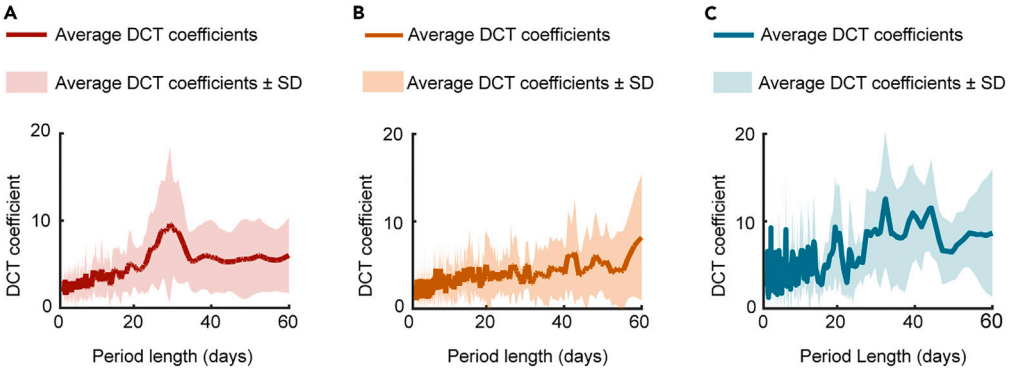

Figure 1. The heart rate of fertile women shows a monthly rhythm

(A) Average periodogram across all fertile women (N = 91) shows monthly rhythm (peak at 29.27 days). Shade indicates DCT coefficient ± SD.

(B and C) Average periodogram across all menopausal women (N = 12) and all men (N = 15), respectively.

RESULTS

Fertile women display a monthly rhythm of heart rate

To investigate the connection between heart rate and menstrual cycle, we recruited a group of fertile women (24.44 ± 2.84), men (38.80± 10.82), and menopausal women (57.08± 5.44) (as described in the STAR Methods) and collected minute-level heart rate using wearable devices (Figure S1A). To exclude the effects of daytime activities, emotions, and unexpected events, we calculated the average heart rate during the rest period at night (Figures S1B and S2). We also conducted a spectral analysis, discrete cosine transform (DCT) (as described in the STAR Methods), to examine the regularity of the daily average heart rate. The average daily heart rate of each participant was analyzed by DCT to obtain the coefficient curve. To obtain generalizable results, we statistically analyzed the coefficient curves for all fertile women, all men, and all menopausal women. Figure 1 illustrates the average DCT coefficient curves (line) and the range of standard deviations (shading) of the coefficient curves for the three groups. The results revealed that fertile women have a regular monthly rhythm of heart rate, with a pronounced peak occurring approximately every 30 days (Figure 1A). Importantly, this period feature was not observed in menopausal women and men (Figures 1C and 1D). These results suggest that monthly rhythm of heart rate is a robust feature of the menstrual cycle in fertile women.

The velocity trajectory correlates with the menstrual cycles

Since the heart rates of fertile women show a prominent monthly rhythm, we further explored their characteristics within menstrual cycles. Before further data processing, the daily average heart rate did not show an ovulatory signature. The graph clearly shows that ovulation does not occur at the peak or trough of the daily average heart rate (Figure S3A). Statistical analysis showed a lack of correlation between ovulation and the distance to peak or trough (Figure S3B), implying that the daily average heart rate itself cannot serve as an early warning sign for ovulation. We further supplemented the missing data with linear interpolation and smoothed the heart rate using Butterworth low pass filtering with appropriate filtering parameters (as described in the STAR Methods). Ovulation occurs at the low-to-high part of the heart rate, and menstruation occurs at the decreasing heart rate (Figure S4A), but it was still difficult to distinguish ovulation from menstruation based on the heart rate values (Figures S4B and S4C).

Given that the menstrual cycle is governed by multiple feedback loops such as the negative feedback loop of the hypothalamic-pituitary-ovarian axis, inhibitory factors act to inhibit the production of the target molecule by reducing its production rate or increasing its degradation or conversion rate. Therefore, the change rate of the inhibited factor, rather than its absolute level, is a direct reflection of the strength and activity of the inhibitory factor in inhibitory signal transduction.

We thus statistically analyzed the derivative curve, which is a mathematical representation of the rate of change in a variable over time. We found that most of the derivatives at ovulation are greater than 0, and the derivatives at menstruation are less than 0 (Figure S4D), suggesting that the derivative curve is more likely to reflect the characteristics of the menstrual cycle. In Figure 2A, the derivative curve of one subject is presented, indicating that the ovulation was approximately at the peaks and menstruation was approximately at the troughs of the curve. The violin plot shows that the distances between ovulation and the peaks of the derivative curves are distributed in a relatively narrow range (Figure 2B). There are 65.79% of the ovulations distributed within the 7-day span of the peak (three days before to three days after). The distances between menstruation and troughs are also in a relatively narrow range, and 70.83% of the menstruation is in the 7-day span around the troughs (Figure 2B). This result indicates that the extreme points of the derivative curve may serve as a biomarker for menstruation and ovulation.

The maximum velocity corresponds to the menstrual cycle transition

We aim to investigate whether the maximum value points of the velocity can serve as critical points for ovulation. It is well known that individuals can differ in their physiological characteristics and responses. This can result in variations in the lengths of the menstrual cycle, as well

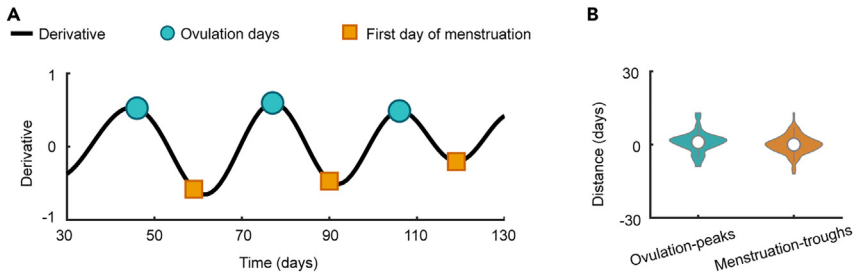

Figure 2. The day of ovulation and the first day of menstrual bleeding correspond to the peak and trough of the velocity trajectory of the heart rate, respectively

(A) The velocity trajectory (derivative) of the heart rate of one subject is presented.

(B) Two violin plots demonstrate the distribution of the distance between the peak and ovulation and the distance between the trough and the first day of menstruation on the velocity trajectory of the heart rate.

as the amplitudes of the heart rate signal between individuals. Therefore, it is important to adjust for normalizing the menstrual cycle to 28 days[17] The flowchart illustrated in Figure S5 outlines our approach. To investigate the correlation between ovulation and the peaks of the velocity profile, we divided the curve into cycles at the trough of the derivative curve and rescaled them to a standard 28-day length. Upon averaging all cycles, we discovered that ovulation occurred at the peak of the derivative curve (Figure 3A). Furthermore, the relationship between the peak of the derivative curve and ovulation still exists across different individuals, despite variations in their menstrual cycle lengths (Figures 3B and 3C). If a calendar-based method is used to predict ovulation in cycles with irregular length, the estimation of ovulation time is highly inaccurate. This suggests that the early warning signal is not dependent on the specific physiological characteristics of each individual but rather reflects a more general physiological response.

In real-time prediction, using the maximum value of the first-order derivative as a direct criterion presents challenges. This is due to the difficulty in determining whether the maximum value has been reached in the absence of subsequent data. One approach is to employ machine learning techniques to train the prediction system to identify indicative features associated with extreme values of the first-order derivative. Inputs such as the first-order derivative itself (rather than the extreme value), as well as the second-order derivative (whose approach to 0 can reflect the emergence of the extreme value), can be used to train the system, as the tendency for the extreme value to emerge is often embedded in these data. However, our study is constrained by data limitations. We have established that first-order derivative maxima can serve as a biomarker for ovulation, but further data are essential to train a comprehensive predictive model capable of real-time forecasting. In addition, some existing prediction methods, such as Kalman filtering, can be considered for predicting the subsequent heart rate trend to determine the extreme value of the first-order derivative.

The amplitude of oscillation is required for the accuracy of biomarkers

External factors such as environment, emotional stress, and illness can influence both ovulation and heart rate, which may affect the accuracy of using heart rate as a biomarker. Because the robustness, especially the amplitude, of oscillation is a critical characteristic of oscillatory systems, it is hypothesized that the derivative feature of stronger oscillations is more accurate for detecting the early warning signal for ovulation. To investigate the relationship between heart rate amplitude and ovulation position, we first studied several cases. The accuracy of the biomarker for different amplitude scenarios is demonstrated in Figures 4A–4F. Figure 4A illustrates a cycle with a higher amplitude of heart rate (7.13) and a distance of −1 day between ovulation and the peak of the derivative (Figure 4D). In contrast, Figure 4B depicts a cycle with a lower amplitude (3.87) and a distance of 3 days between ovulation and peak (Figure 4E), which is larger than that of Figure 4D. Figure 4C shows a case where the amplitude (1.09) is particularly small, and ovulation occurs far from the peak of the derivative.

We then conducted a statistical analysis to further investigate the relationship between heart rate amplitude and ovulation position. In Figure 4G, the green dots represent the relationship between the amplitudes and the distances of ovulation position in all cycles. These dots indicate a negative correlation between the amplitude and distance, meaning that, the larger the amplitude, the smaller the distance tends to be. The spearman correlation coefficient is −0.2894 with a p value of 0.0665. We computed the average values for data points below- and above-zero distance, with an amplitude interval of 1.5 for each set (dotted lines in Figure 4G). The Spearman correlation coefficient for the absolute value of these average values is − 0.9762, and the p value is 3.97×10^{-4}. These results demonstrate that the distance between ovulation and peak tends to decrease as the amplitude increases. It implies that the effectiveness of the biomarker highly depends on the oscillatory ability of the system. Thus, the amplitude of the oscillations is a critical factor in ensuring the accuracy of ovulation prediction.

The maximum velocity of calcium signaling in the SCN coincides with the locomotor offset

Given that biological oscillations typically share a similar driving mechanism, it is uncertain whether a similar biomarker relying on derivatives can be applied to other endogenous biological rhythms. One of the most prevalent rhythmic oscillations is the circadian rhythm, which is observed in various aspects of cellular physiology, such as intracellular calcium signals[18] and electronic signals.[19] To investigate further, we analyzed an additional set of experimental data obtained from a circadian rhythm study.[20,21]

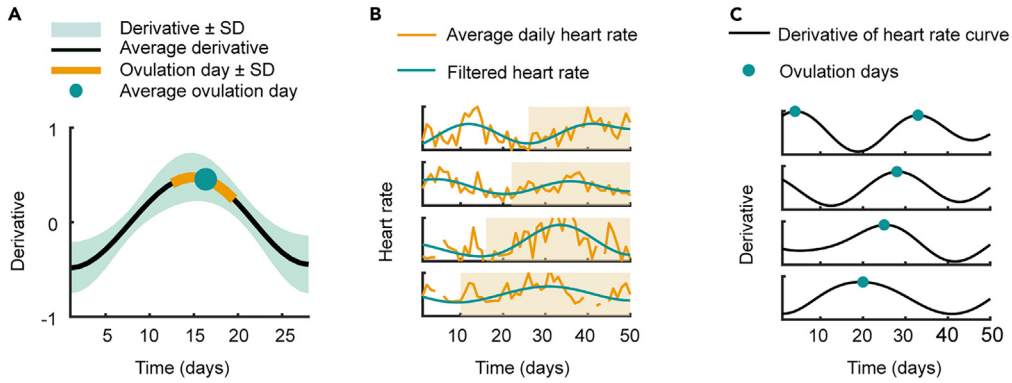

Figure 3. Ovulation corresponds to the peak of the velocity trajectory of the heart rate and applies to different cycle lengths

(A) Divide the velocity trajectory of the heart rate curve into cycles at the troughs and rescale all divided cycles into 28 days. The blue curve is the average of all derivatives of the heart rate curves for all cycles, and the average ovulation day is approximately at the maximum of this curve.

(B) Four menstrual cycles (shaded areas) with different lengths, which are 24, 29, 35, and 41 days, respectively.

(C) The derivative curves and ovulation markers correspond to the cycles in Figure 3B.

In the experiment, we analyzed two sets of data: Ca^{2+} signals in the SCN (Figure 5B) and activity (Figure 5A) in mice.[20,21] The mice exhibited a locomotor circadian rhythm (Figure 5A), while the SCN presented spontaneous calcium oscillations (Figure 5B). We filtered the calcium signals of four mice and found that the mean time of the activity offset coincided with the rising part of the calcium signal (Figure 5C). Next, we normalized and averaged all filtered calcium signals to obtain the mean derivative curve. The transition point of activity in mice was located approximately at the peak of the derivative curve (Figure 5D), which is similar to the correlation between ovulation and heart rate. Furthermore, this correlation is also present between SCN electrical signals and mouse activity.[19]

The characteristics of the calcium signal and the electrical signal suggest that the maximum values of the rate of change, as a biomarker for transition points, may not be specific to monthly rhythms alone and could potentially be applicable to other endogenous biological rhythms that are governed by negative feedback oscillations.

The maximum of the derivative has the potential to serve as a universal biomarker

In the preceding sections, we examined how monthly and circadian rhythms share the feature of exhibiting maximum derivatives as biomarkers for behavioral transitions. This led us to question the underlying mechanisms responsible for these similarities and whether they extend to other domains. Negative feedback is a well-known driver of many biological oscillations, including the classic circadian rhythm oscillator. Other biological oscillations, such as the oscillations of p53 in response to ionizing radiation[22] and the oscillations of nuclear factor κ B (NF-κ B) in response to stimulation by tumor necrosis factor,[23] also rely on negative feedback, although their regulatory networks may involve complex positive feedback and other forms of regulation. Likewise, the regulation of the menstrual rhythm is complex, with both positive and negative feedback playing critical roles in the hypothalamic-pituitary-ovarian axis. Therefore, we propose that negative feedback could be the fundamental factor behind the derivative biomarkers in these biological oscillations.

We delved deeper into the biomarker of negative feedback oscillators through a mathematical model. We proposed a simplified 3-component conceptual model that captures the essential mechanism of negative feedback oscillators. In this model, variable x activates y, which activates z, and z, in turn, exerts negative feedback to inhibit x (Figure 6A). In the negative feedback loop, z acts as the inhibitory factor, and x is the inhibited factor. The model incorporates Hill function terms to describe the dynamics of x, y, and z. The ordinary differential equations for the three variables are

$$\frac{dx}{dt} = k_1 \cdot \frac{K_1^{n_1}}{K_1^{n_1} + z^{n_1}} - k_{d_1} \cdot x \qquad \text{(Equation 1)}$$

$$\frac{dy}{dt} = k_2 \cdot \frac{x^{n_2}}{K_2^{n_2} + x^{n_2}} - k_{d_2} \cdot y \qquad \text{(Equation 2)}$$

$$\frac{dz}{dt} = k_3 \cdot \frac{y^{n_3}}{K_3^{n_3} + y^{n_3}} - k_{d_3} \cdot z \qquad \text{(Equation 3)}$$

In this model, the Hill function $\frac{K_1^{n_1}}{K_1^{n_1}+z^{n_1}}$ represents the inhibition of z on x, $\frac{x^{n_2}}{K_2^{n_2}+x^{n_2}}$ represents the promoting effect of x on y, $\frac{y^{n_3}}{K_3^{n_3}+y^{n_3}}$ is the promoting term of y on z, k_i $(i = 1, 2, 3)$ represents the maximum production rate, n_i $(i = 1, 2, 3)$ represents the Hill coefficient, and k_{di} $(i = 1, 2, 3)$ represents the degradation rate. This model can be applied to describe the core negative feedback in various biological oscillations. To investigate whether the derivative of x could serve as an indicator of the turning point of z, as observed in the biomarker of monthly and circadian rhythms, we explored the model further.

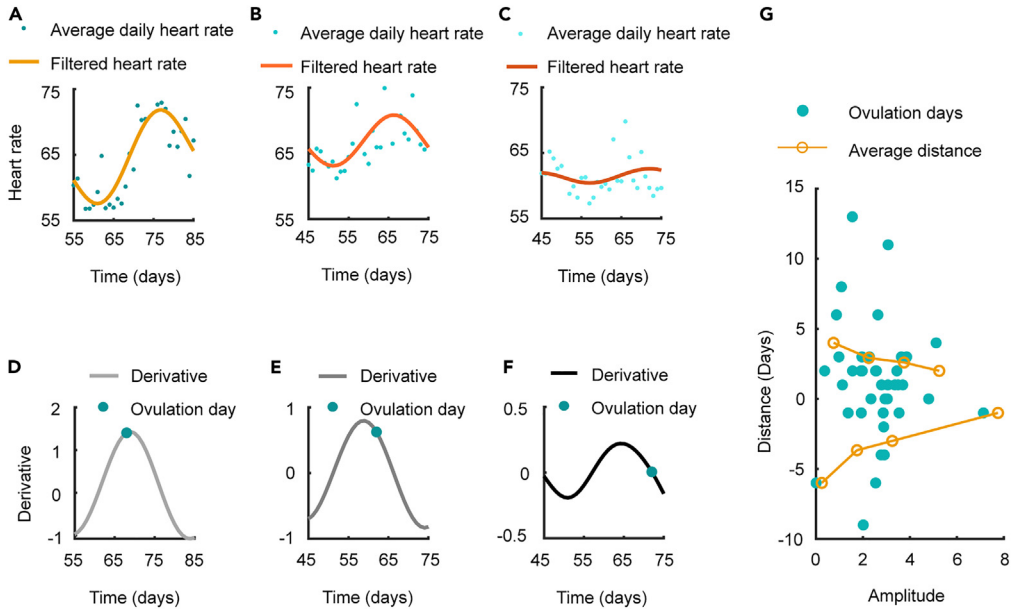

Figure 4. The distances between the ovulation and the derivative maxima decreas as the heart rate amplitude increases

(A–C) Heart rates from three different subjects, with different amplitudes of the heart rates.

(D–F) The derivative curves corresponding to the heart rate shown in Figures 4A–4C. The ovulation marker is farther away from the maximum value as the amplitude increases.

(G) The greater the heart rate amplitude, the closer the distance between ovulation and the maximum value of the heart rate derivative. The two red lines represent the average distance, in amplitude increments of 1.5, from ovulation to the peak of the derivative. The positive and negative distances distinguish between ovulation to the left or right of the peak.

The menstrual cycle involves complex physiological phenomena and intrinsic mechanisms that require the multifaceted interaction of hormones and organs through the hypothalamic-pituitary-ovarian axis (Figure S6A). The hypothalamus releases pulsatile gonadotropin-releasing hormones, which stimulate the pituitary gland to produce gonadotropins (follicle-stimulating hormone [FSH] and luteinizing hormone [LH]). These gonadotropins promote the secretion of ovarian steroids (estradiol, progesterone) and non-steroids (inhibin A, inhibin B, and gonadotropin surge-attenuating factor [GnSAF], etc.), which are essential components of the negative feedback mechanism. Various studies have modeled the menstrual cycle from different perspectives, such as the intrinsic mechanism that triggers the LH surge,[24] description of the dynamics of hormones, enzymes, receptors, and follicles,[25] the model of gonadotropin hormone-releasing hormone [GnRH] receptor binding,[26] the model of ovarian reserve capacity,[27] and the pulsatile secretion of hypothalamic and pituitary hormones from a cellular endocrine perspective.[28] In this study, we focus on one of the key negative feedbacks in the hypothalamic-pituitary-ovarian axis as a driving force of the oscillation. Using the model described by Equations 1, 2, and 3, we describe the feedback loop of the menstrual cycle, with variables x, y, and z representing the GnRH, FSH/LH, and GnSAF secreted by the hypothalamus, pituitary gland, and ovaries, respectively (Figure S6B).

In the model, the variable z represents the hormone secreted by the ovary that inhibits the secretion or function of hypothalamic hormones. For example, the hormone GnSAF, produced by the ovary, inhibits the function of GnRH, which in turn stimulates the release of gonadotropins (Figure S6B). GnSAF levels decrease during the follicular phase and rise in the late luteal phase.[29] During the transition phase between the follicular and luteal phases, GnSAF is at a low level, and there is a surge of LH at this time. Therefore, ovulation occurs at the trough of the variable z in the model. Additionally, heart rate, which is regulated by the hypothalamus,[30–32] is represented in the model by variable x. As a result, the relationship between heart rate and ovulation, as demonstrated in the menstrual cycle data, is reflected in the model as the relationship between the derivative of x and the turning point of z.

Circadian rhythm is a fundamental biological rhythm that is driven by negative feedback loops. In mammalian, CLOCK and BMAL are proteins involved in the regulation of circadian rhythms. The unbound CLOCK-BMAL protein activates the *Per* (period) and *Cry* (cryptochrome) genes, facilitating their transcription into mRNA and producing the protein complex PER-CRY. By binding to the CLOCK-BMAL complex, PER-CRY exerts an inhibitory effect on the transcriptional activation of the *Per* and *Cry* genes by CLOCK-BMAL (Figure S6C).[33] The CLOCK-BMAL and PER-CRY negative feedback loop is the key driving force of the mammalian circadian rhythm. When using the model (Equations 1, 2, and 3) to describe the feedback loop of circadian rhythm, the variables x, y, and z represent CLOCK-BMAL, mRNA of *Per-Cry* genes, and PER-CRY, respectively (Figure S6D). As the calcium signal is correlated with CLOCK-BMAL (x),[34,35] the calcium signal can represent x. Based on the experimental results, the position where the calcium signal increases fastest corresponds to the turning point of the activity. Therefore, the maximum value of the derivative of x can serve as a biomarker of activity in circadian rhythms.

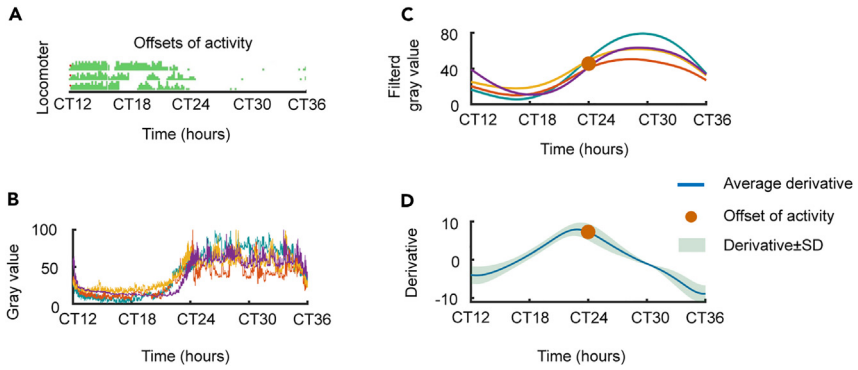

Figure 5. Transition points of activity on circadian rhythms are correlated with the maximum velocity trajectory

Mice were first entrained under 12 h:12 h light-dark cycles for 2 weeks. Then, wheel activity and Ca^{2+} signals were recorded under dark conditions.

(A) One representative actogram of wheel running was aligned to the Ca^{2+} signals in Figure 5B. CT12 corresponds to subjective dusk, and CT24 corresponds to subjective dawn.

(B) The intracellular Ca^{2+} signals (fluorescence intensity normalized to 0 to 100) in the SCN of four mice.

(C) Filtering of the calcium signal in Figure 5B.

(D) The average of the derivatives of the curves in Figure 5C.

Therefore, we conducted numerical simulations to verify that the maximum value of the derivative of x can serve as a biomarker in negative feedback-driven oscillators, as observed in biological experiments. We explored a large number of randomly selected parameter sets in the 3-variable negative feedback model (Equations 1, 2, and 3) using computational methods. Specifically, we sampled 100,000 parameter sets uniformly in the parameter space on a logarithmic scale using the Latin hypercube sampling method.[36] The parameters were sampled in the range $k_i \sim 10^{-2} - 10^3$, $K_i \sim 10^{-2} - 10^3$, $k_{di} \sim 10^{-2} - 10^3$, $n_i \sim 1 - 10$ (integer), $i = 1, 2, 3$. In oscillatory systems, we defined the relative phase difference between the maximum value of the derivative of x and the minimum value of z (indicates the phenotype transition) as $\Delta\varphi = d_1 / d_2$, where d_1 is the closest distance between the peak point of the derivative of x and the trough of z and d_2 is the period length (Figure 6B). Out of these parameter sets, 1,229 sets of parameters could generate oscillations, and of those, 92.6% had a $\Delta\varphi$ of less than 10% (Figure 6C). This indicates that when a system is capable of oscillating, it is natural for the phase difference ($\Delta\varphi$) to be relatively small (<10%), meaning that the maximum point of the derivative of x is close to the turning point of z in most parameter sets. This result is consistent with experimental data in which ovulation is located at the maximum of the heart rate derivative, thus validating the proposed biomarker of ovulation.

We further investigated why most of the oscillations have a small relative phase difference between the maximum value of the derivative of x and the minimum value of z, regardless of the parameters. The menstrual cycle data show a negative correlation between the oscillatory ability of the system and the phase difference (Figure 4), as it suggests that the strength of negative feedback is crucial for accuracy of the biomarker. Thus, we analyzed the inhibited factor metabolism index (*IFM*) measured as k_1/k_{d1} in the 1,229 sets of oscillations, where k_1 represents the production of the suppressed factor and k_{d1} represents its degradation rate. First, within the oscillatory systems, we found that the average *IFM* value is 1603.8559 and the proportion of *IFM* values greater than 1 constitutes 84.54% of the distribution. In the non-oscillatory systems, the average *IFM* value is 748.5009, and the proportion of *IFM* values exceeding 1 is 49.61% (Figure 7A). These results suggest that the generation of oscillations requires the relatively large *IFM*. Then, our results show a consistent negative relationship between negative feedback strength and $\Delta\varphi$ (Figure 7B). The earlier analysis demonstrates that the generation of system oscillations requires a relatively large *IFM*, which corresponds to a small $\Delta\varphi$. Furthermore, if the system has a strong oscillation capacity, the early warning points presented previously will naturally exhibit higher accuracy.

Using one of the parameters sets as a case study, we further demonstrated the link of oscillation ability - large *IFM* — $\Delta\varphi$. The bifurcation diagram shows that, as *IFM* decreases, the system undergoes a Hopf bifurcation ($\log_{10}(NFS) \approx 1.0398$): from a stable limit cycle to the non-oscillatory steady state (Figure 7C). Figure 7D illustrates how the amount of x varies (indicated by colors) along the time under different *IFM*. When $\log_{10}(IFM)$ is more than 1.0398, the system oscillates and has a stable limit cycle. For instance, point a in Figure 7C represents the unstable steady state when $\log_{10}(IFM) = 1.5$, while points b and c represent the maximum and minimum points of the system oscillation, respectively. At $\log_{10}(IFM) = 1.5$, the color of x varies periodically with time due to the oscillation (Figure 7D). However, when $\log_{10}(IFM)$ decreases and crosses 1.0398, the steady state becomes stable, and the oscillation disappears. When $\log_{10}(IFM) = 0.8$, point d in Figure 7C represents a stable steady state and the color of x remains constant, indicating a non-oscillatory system (Figure 7D). This case shows that the oscillating system requires a relatively large negative feedback strength; otherwise the system cannot oscillate. Our numerical simulation results also display a negative correlation between *IFM* and $\Delta\varphi$ (Figure 7E), indicating that, when the negative feedback strength of the system reaches a certain level, it turns from non-oscillatory to oscillatory, and $\Delta\varphi$ decreases. Since oscillating systems are typically associated with relatively large *IFM*, small $\Delta\varphi$ is implied. Therefore, when the system is oscillating, $\Delta\varphi$ will be small, and the peak point of the derivative of x will be close to the turning point of the physiological activity.

We also found that the amplitude (half of the difference between the maximum and minimum values of x) of the oscillation increases with *IFM* (Figure 7C), while $\Delta\varphi$ and the amplitude of the system show a negative correlation (Figure 7F). This finding is consistent with our

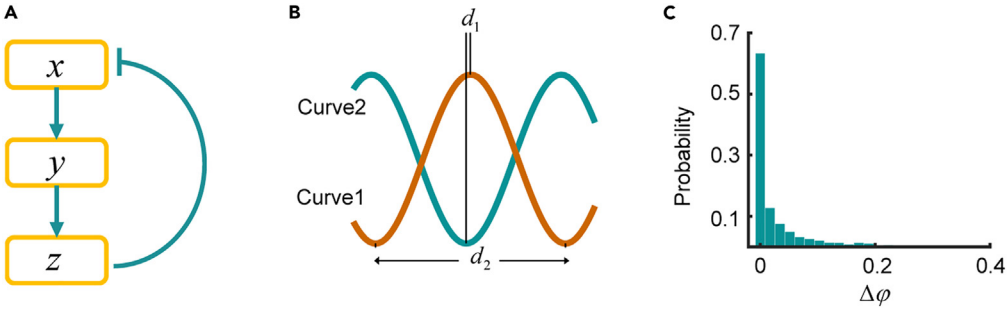

Figure 6. Negative feedback loops that can oscillate have a relatively small $\Delta\varphi$

(A) Negative feedback loop for biological oscillations.

(B) Definition of the $\Delta\varphi$. $\Delta\varphi$ is defined as d_1/d_2, where d_1 is the closest distance between the peak of curve1 and the trough of curve2 and d_2 is the period length.

(C) Distribution of $\Delta\varphi$ of the 1,229 oscillating systems. The vertical coordinate indicates the proportion of the number of different $\Delta\varphi$ in all oscillations.

experimental results (Figure 4) that higher amplitude oscillations lead to a more accurate biomarker. Thus, in a robust oscillating system, the location of the maximum value of the derivative of *x* can serve as a marker for the turning point of physiological activity.

DISCUSSION

Our study reveals that the peak value of the derivative of the daily average heart rate can serve as a reliable biomarker of ovulation. Additionally, we observed a distinct monthly rhythmicity in the daily average heart rate of women of reproductive age using DCT analysis. However, the daily average heart rate curves and smoothed curves did not clearly reflect ovulation. We found that the characteristics of the heart rate during ovulation may be reflected in the positive derivatives of the daily average heart rate curves, which were observed to be in the ascending phase on the day of ovulation. Statistical analysis revealed that the point of the maximum value on the derivative curve of the heart rate corresponds to the day of ovulation, even in irregular cycles, making this feature of the heart rate a valuable marker for ovulation. Furthermore, menstrual cycles with higher heart rate amplitude exhibit biomarkers with greater accuracy.

Our study highlights the potential of using derivatives of upstream signals as biomarkers for critical transitions in downstream activity, not only in the context of monthly rhythms but also in circadian rhythms. Our experiments demonstrated that the maximum value point of the calcium signal derivative in the SCN is correlated with the offset point of running wheel activity in mice. Similarly, a study[19] showed that the maximum value point of the electrical signal derivative in the SCN is correlated with the offset point of mouse activity. These findings suggest that the extreme value of the derivative point can serve as a valuable biomarker for identifying the transition point of physiological activity, with broader implications beyond monthly rhythms.

Finally, we developed a mathematical model that incorporates negative feedback loops and conducted a random parameter search to verify the robustness of the maximum value point of the derivative as a marker for turning points. Out of 100,000 sets of stochastic parameters tested, 1,229 were found to be oscillatory. Statistical analysis showed that, in over 90% of the oscillatory systems, the maximum value of the derivative of the variable *x* was close to the minimum value of the variable *z*, suggesting that the peak point of the derivative of *x* can be used as a reliable marker of the turning point of *z* as long as the system is oscillatory. Importantly, this marker is independent of parameters and thus generalizable. Our analysis also revealed that oscillatory systems are accompanied by stronger negative feedback, and this negative feedback strength is negatively correlated with the phase difference between the peak of the derivative of variable *x* and the trough of variable *z*. Therefore, a small phase difference is naturally observed as long as the system is oscillating. These findings support the universality of this marker for identifying turning points in a broad range of oscillatory systems.

Additionally, this biomarker may have practical applications in healthcare, such as predicting the onset of disease or monitoring disease progression. For example, in cardiovascular disease, changes in heart rate variability have been linked to disease progression and outcomes.[16] The biomarker we proposed could potentially be used to monitor changes in heart rate and predict disease onset or progression. Furthermore, it could be used in personalized medicine to optimize drug dosing based on the timing of physiological activity in individual patients. Overall, while further validation is necessary, the potential applications of this biomarker are promising and warrant further investigation.

Importantly, our proposed biomarker may have clinical applications for couples undergoing fertility treatment. In assisted reproductive technologies (ARTs), the precise timing of ovulation is critical for successful outcomes. The use of our biomarker in combination with other predictive methods may increase the chances of success in ART procedures. Furthermore, for women who are trying to conceive naturally, our biomarker could help increase the chances of successful conception by identifying the optimal time for intercourse. Overall, the use of our biomarker has the potential to improve the accuracy and effectiveness of ovulation prediction and fertility treatment, ultimately leading to better reproductive health outcomes for women.

Using the maximum points of the derivatives can improve the accuracy of inferring inhibition relationships in oscillatory systems because it captures the turning points of downstream activity, which may not align with the static levels of upstream signals. By identifying the maximum points of the derivatives of variables in an oscillatory system, we can infer the inhibition relationship between them. For example,

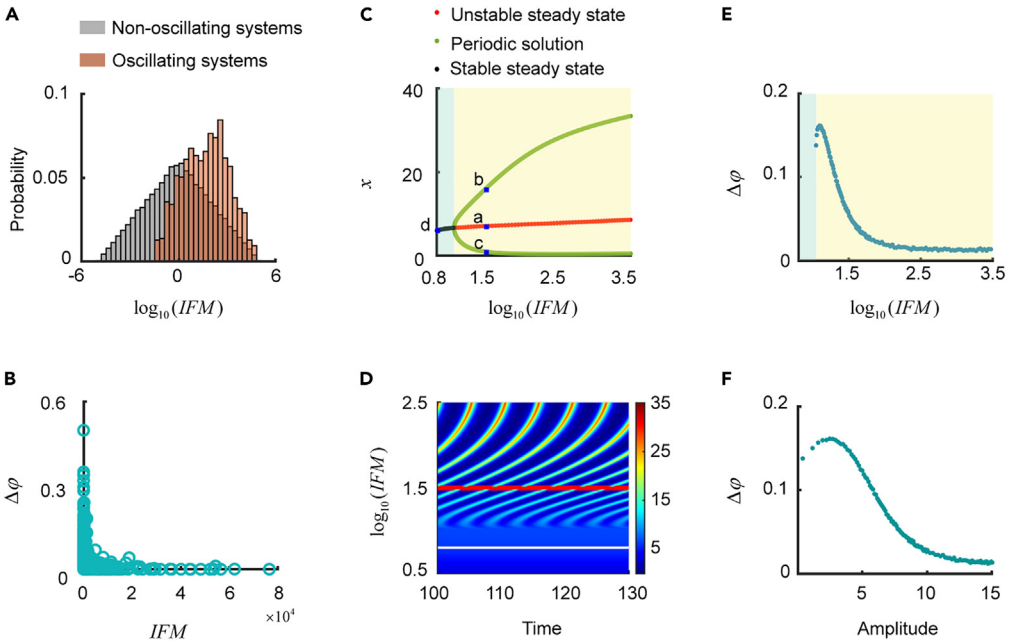

Figure 7. The maximum of the derivative has the potential to serve as a universal biomarker

(A) Negative feedback strength distributions for 1,229 oscillating systems and non-oscillating systems. The proportion of *IFM* values greater than 1 constitutes 84.54% of the overall distribution within the oscillatory system, whereas within the non-oscillatory system the proportion of *IFM* values exceeding 1 is 49.61%.

(B) In the statistical analysis of the 1,229 groups of oscillations, a significant negative correlation between $\Delta\varphi$ and *IFM* was observed.

(C) The bifurcation diagram. The parameters are $n_1 = 4$, $n_2 = 2$, $n_3 = 4$, $K_1 = 0.71679$, $K_2 = 15.0947$, $K_3 = 30.3943$, $k_2 = 34.2662$, $k_3 = 51.8191$, $k_{d_1} = 1.6952$, $k_{d_2} = 0.63577$, and $k_{d_3} = 0.59482$. The system of ordinary differential equations was solved using the XPPAUT software for computation.

(D) The heatmap depicts multiple sets of *x* time series (indicated by color) from non-oscillating to oscillating, at different *IFM* (ordinates). Each different *IFM* corresponds to a time series of *x*.

(E) Under the parameters of Figure 7C, $\Delta\varphi$ decreases as *IFM* increases.

(F) Changing the range of k_1 in a set of parameters; the larger the amplitude, the smaller the $\Delta\varphi$.

in a gene regulatory network, the maximum point of the derivative of a repressor gene may correspond to the activation of its target gene. This method can potentially provide a more accurate representation of the network's regulatory interactions, particularly in dynamic systems.

Limitations of the study

One limitation of the study is that we did not employ aforementioned biomarkers directly for prediction in this work due to the restricted amount of valid data. Some individuals were unable to wear their bracelets consistently every day during the heart rate data collection, which resulted in a significant number of missing values in the obtained data and a decrease in the amount of valid data.

STAR★METHODS

Detailed methods are provided in the online version of this paper and include the following:

- KEY RESOURCES TABLE
- RESOURCE AVAILABILITY
  - Lead contact
  - Materials availability
  - Data and code availability
- EXPERIMENTAL MODEL AND STUDY PARTICIPANT DETAILS
  - Menstrual cycle data
  - Circadian rhythm data
- METHOD DETAILS
  - Extract daily average heart rate from minute-level heart rate during resting phase
  - Missing value processing

- DCT analysis
- Average daily heart rate smoothing
- Calcium signal data processing

- QUANTIFICATION AND STATISTICAL ANALYSIS

SUPPLEMENTAL INFORMATION

Supplemental information can be found online at https://doi.org/10.1016/j.isci.2023.108716.

ACKNOWLEDGMENTS

We thank Zhirong Yuan for his support in data preprocessing. We are also grateful to all participants who recorded their heart rate and menstrual cycle.

This work was supported by the National Key Research and Development Program of China (2018YFA0801100), the National Natural Science Foundation of China (12071330, 31630091), the State Scholarship Fund of China Scholarship Council, the Science and Technology Project of Jiangsu Province (BZ2020067), the Priority Academic Program Development of the Jiangsu Higher Education Institutes, and the Lingang Laboratory & Nationa Key Laboratory of Human Factors Engineering Joint grant LG-TKN-202203-01.

AUTHOR CONTRIBUTIONS

L.Y. and Y.X. conceived and designed the research; Y.W., L.Y., and Y.X. developed and implemented methodologies; Y.D. collected heart rate data and data related to the female menstrual cycle; and Q.Z. provided data related to activity and calcium signaling in mice. Y.W. performed data analysis and data visualization. Y.W. and W.Z. preprocessed the heart rate data. Y.W., Y.X., and L.Y. wrote the manuscript. L.Y. and Y.X. supervised the whole research process.

DECLARATION OF INTERESTS

The authors declare no competing interests.

Received: July 26, 2023
Revised: October 13, 2023
Accepted: December 11, 2023
Published: December 13, 2023

REFERENCES

1. Patke, A., Young, M.W., and Axelrod, S. (2020). Molecular mechanisms and physiological importance of circadian rhythms. Nat. Rev. Mol. Cell Biol. *21*, 67–84.
2. Raible, F., Takekata, H., and Tessmar-Raible, K. (2017). An overview of monthly rhythms and clocks. Front. Neurol. *8*, 189.
3. Korf, H.W. (2018). Signaling pathways to and from the hypophysial pars tuberalis, an important center for the control of seasonal rhythms. Gen. Comp. Endocrinol. *258*, 236–243.
4. Messinis, I.E. (2006). Ovarian feedback, mechanism of action and possible clinical implications. Hum. Reprod. Update *12*, 557–571.
5. Murray, C.M., and Orr, C.J. (2019). Hormonal regulation of the Menstrual Cycle and Ovulation. In Maternal-Fetal and Neonatal Endocrinology: Physiology, Pathophysiology, and Clinical Management, C.S. Kovacs and C. Deal, eds. (Academic Press), pp. 159–167.
6. Welt, C.K. (2004). Regulation and function of inhibins in the normal menstrual cycle. Semin. Reprod. Med. *22*, 187–193.
7. Fowler, P.A., Sorsa-Leslie, T., Harris, W., and Mason, H.D. (2003). Ovarian gonadotrophin surge-attenuating factor (GnSAF): where are we after 20 years of research? Reproduction *126*, 689–699.
8. Messinis, I.E., Messini, C.I., and Dafopoulos, K. (2014). Novel aspects of the endocrinology of the menstrual cycle. Reprod. Biomed. Online *28*, 714–722.
9. Beshay, V.E., and Carr, B.R. (2017). Hypothalamic-pituitary-ovarian axis and control of the menstrual cycle. In Clinical reproductive medicine and surgery: A practical guide, T. Falcone and W. Hurd, eds. (Springer), pp. 1–17.
10. Brar, T.K., Singh, K.D., and Kumar, A. (2015). Effect of different phases of menstrual cycle on heart rate variability (HRV). J. Clin. Diagn. Res. *9*, CC01–CC04.
11. Dunne, F.P., Barry, D.G., Ferriss, J.B., Grealy, G., and Murphy, D. (1991). Changes in blood pressure during the normal menstrual cycle. Clin. Sci. *81*, 515–518.
12. Fukaya, K., Kawamori, A., Osada, Y., Kitazawa, M., and Ishiguro, M. (2017). The forecasting of menstruation based on a state modeling of basal body temperature time series. Stat. Med. *36*, 3361–3379.
13. Goodale, B.M., Shilaih, M., Falco, L., Dammeier, F., Hamvas, G., and Leeners, B. (2019). Wearable sensors reveal menses-driven changes in physiology and enable prediction of the fertile window: observational study. J. Med. Internet Res. *21*, e13404.
14. Valentini, M., and Parati, G. (2009). Variables influencing heart rate. Prog. Cardiovasc. Dis. *52*, 11–19.
15. Brandman, O., and Meyer, T. (2008). Feedback loops shape cellular signals in space and time. Science *322*, 390–395.
16. Zhang, T., Du, X., Gu, Y., Dong, Y., Zhang, W., Yuan, Z., Huang, X., Zou, C., Zhou, Y., Liu, Z., et al. (2022). Analysis of Diurnal Variations in Heart Rate: Potential Applications for Chronobiology and Cardiovascular Medicine. Front. Physiol. *13*, 835198.
17. Cole, L.A., Ladner, D.G., and Byrn, F.W. (2009). The normal variabilities of the menstrual cycle. Fertil. Steril. *91*, 522–527.
18. Noguchi, T., Leise, T.L., Kingsbury, N.J., Diemer, T., Wang, L.L., Henson, M.A., and Welsh, D.K. (2017). Calcium circadian rhythmicity in the suprachiasmatic nucleus: Cell autonomy and network modulation. Eneuro *4*. ENEURO.0160-17.2017.
19. Houben, T., Deboer, T., van Oosterhout, F., and Meijer, J.H. (2009). Correlation with behavioral activity and rest implies circadian regulation by SCN neuronal activity levels. J. Biol. Rhythm. *24*, 477–487.
20. Zhai, Q., Zeng, Y., Gu, Y., Li, Z., Zhang, T., Yuan, B., Wang, T., Yan, J., Qin, H., Yang, L., et al. (2022). Time-restricted feeding entrains long-term behavioral changes through the IGF2-KCC2 pathway. iScience *25*, 104267.
21. Zhai, Q., Zeng, Y., Li, Z., Xu, Y., and Xu, Y. (2022). Long-term SCN calcium signal recording in freely moving mice. STAR Protoc. *3*, 101547.

22. Lev Bar-Or, R., Maya, R., Segel, L.A., Alon, U., Levine, A.J., and Oren, M. (2000). Generation of oscillations by the p53-Mdm2 feedback loop: a theoretical and experimental study. Proc. Natl. Acad. Sci. USA *97*, 11250–11255.
23. Cheong, R., Hoffmann, A., and Levchenko, A. (2008). Understanding NF-κB signaling via mathematical modeling. Mol. Syst. Biol. *4*, 192.
24. Zeeman, M.L., Weckesser, W., and Gokhman, D. (2003). Resonance in the menstrual cycle: a new model of the LH surge. Reprod. Biomed. Online *7*, 295–300.
25. Reinecke, I., and Deuflhard, P. (2007). A complex mathematical model of the human menstrual cycle. J. Theor. Biol. *247*, 303–330.
26. Röblitz, S., Stötzel, C., Deuflhard, P., Jones, H.M., Azulay, D.O., van der Graaf, P.H., and Martin, S.W. (2013). Mathematical model of the human menstrual cycle for the administration of GnRH analogues. J. Theor. Biol. *321*, 8–27.
27. Xu, H., Feng, G., Wang, H., Han, Y., Yang, R., Song, Y., Chen, L., Shi, L., Zhang, M.Q., Li, R., and Qiao, J. (2020). A novel mathematical model of true ovarian reserve assessment based on predicted probability of poor ovarian response: a retrospective cohort study. J. Assist. Reprod. Genet. *37*, 963–972.
28. Clément, F., Crépieux, P., Yvinec, R., and Monniaux, D. (2020). Mathematical modeling approaches of cellular endocrinology within the hypothalamo-pituitary-gonadal axis. Mol. Cell. Endocrinol. *518*, 110877.
29. Messinis, I.E., Messini, C.I., Anifandis, G., Garas, A., and Daponte, A. (2018). Gonadotropin surge-attenuating factor: a nonsteroidal ovarian hormone controlling GnRH-induced LH secretion in the normal menstrual cycle. Vitam. Horm. *107*, 263–286.
30. Coote, J.H. (1995). Cardiovascular function of the paraventricular nucleus of the hypothalamus. Neurosignals *4*, 142–149.
31. Blair, M.L., Piekut, D., Want, A., and Olschowka, J.A. (1996). Role of the hypothalamic paraventricular nucleus in cardiovascular regulation. Clin. Exp. Pharmacol. Physiol. *23*, 161–165.
32. Coote, J.H. (2005). A role for the paraventricular nucleus of the hypothalamus in the autonomic control of heart and kidney. Exp. Physiol. *90*, 169–173.
33. Leloup, J.C., and Goldbeter, A. (2003). Toward a detailed computational model for the mammalian circadian clock. Proc. Natl. Acad. Sci. USA *100*, 7051–7056.
34. Kon, N., Yoshikawa, T., Honma, S., Yamagata, Y., Yoshitane, H., Shimizu, K., Sugiyama, Y., Hara, C., Kameshita, I., Honma, K.i., and Fukada, Y. (2014). CaMKII is essential for the cellular clock and coupling between morning and evening behavioral rhythms. Genes Dev. *28*, 1101–1110.
35. Cavieres-Lepe, J., and Ewer, J. (2021). Reciprocal relationship between calcium signaling and circadian clocks: Implications for calcium homeostasis, clock function, and therapeutics. Front. Mol. Neurosci. *14*, 666673.
36. Loh, W.L. (1996). On Latin hypercube sampling. Ann. Stat. *24*, 2058–2080.
37. Ahmed, N., Natarajan, T., and Rao, K.R. (1974). Discrete cosine transform. IEEE Trans. Comput. *100*, 90–93.
38. Selesnick, I.W., and Burrus, C.S. (1998). Generalized digital Butterworth filter design. IEEE Trans. Signal Process. *46*, 1688–1694.

STAR★METHODS

KEY RESOURCES TABLE

REAGENT or RESOURCE	SOURCE	IDENTIFIER
Deposited data		
Calcium signal	Q. Zhai et al.[20]	[Mendeley data]: https://doi.org/10.17632/v58stpfcnm.1
Heart rates of fertile women, men and menopausal women	This paper	[Mendeley data]: https://doi.org/10.17632/v58stpfcnm.1
Ovulation records and menstrual records	This paper	[Mendeley data]: https://doi.org/10.17632/v58stpfcnm.1
Software and algorithms		
Matlab Extract daily average heart rate from resting phase in minute-level heart rate	This paper	[Mendeley data]: https://doi.org/10.17632/v58stpfcnm.1

RESOURCE AVAILABILITY

Lead contact

Further information and requests may be directed to, and will be fulfilled by, the lead contact Ling Yang (lyang@suda.edu.cn).

Materials availability

This study did not generate new unique reagents.

Data and code availability

- Original dataset has been deposited on Mendeley and is publicly available as of the date of publication. Accession numbers are listed in the key resources table.
- The code has been deposited on Mendeley and is publicly available as of the date of publication. Accession numbers are listed in the key resources table.
- Any additional information required to reanalyze the data reported in this paper is available from the lead contact upon request.

EXPERIMENTAL MODEL AND STUDY PARTICIPANT DETAILS

Menstrual cycle data

A total of 91 women with menstrual cycles participated in the study, with an average age of 24.44 (± 2.84). All participants included in this study are individuals of East Asian descent hailing from China. Each participant wore a wristband (Huawei or Fitbit) that could detect continuous heart rate for at least two months to record heart rate. Among them, 84 participants (average age 23.52± 2.81) recorded their menstrual periods each month. And 28 participants (average age 24.00± 1.83) recorded the day of ovulation by using LH ovulation strips, starting from day 8 of the menstrual cycle until positive results were obtained. The study collected a total of 80 ovulation records and 469 menstrual records. Additionally, 12 menopausal women and 15 men were recruited, with the average age of 57.08 (± 5.44) and 38.80 (± 10.82), and the same wristbands were used to collect heart rate data for comparison with women's data.

All participants were recruited during 2018-2020 through online advertisement. Inclusion and exclusion criteria were determined by an online questionnaire and an in-person interview. All subjects provided informed consent. The investigation conforms with the principles outlined in the Declaration of Helsinki and was approved by the ethics Committee of Soochow University (ECSU-201800098).

Circadian rhythm data

The data for the analysis of activity and calcium signaling in mice were acquired from experiments conducted by Q. Zhai et al.[20,21] To represent calcium signals, we utilized grayscale values of fluorescence intensity, which were normalized to a scale ranging from 0 to 100 (Figure 5B). The offsets in mice activity were determined through visual examination of the mice actogram of wheel-running (Figure 5A), following the established method outlined in previous studies.[20,21]

METHOD DETAILS

Extract daily average heart rate from minute-level heart rate during resting phase

The raw data collected by the bracelet consists of continuous minute-level heart rate (Figure S1A). Human heart rate (the number of beats per minute) varies throughout the day, with substantial differences in heart rate amplitude between sleep and wakefulness. During the day, the

heart rate is highly variable due to various activities such as exercise and diet; after falling asleep at night, the heart rate enters a distinctly low and stable phase with minimal variation.

To investigate the relationship between monthly rhythm and heart rate, we extracted the average of the nightly sleep data as the daily average heart rate to exclude the effect of different activities on heart rate (Figure S2). First, due to the unevenness of the data, a fourth-order Butterworth low-pass filter with a normalized cutoff frequency of 1/30 was applied to smooth the heart rate at the minute level. The normalized cutoff frequency *Wn* is a parameter of the function *butter*(*n*, *Wn*) in the MATLAB software, defined as the cutoff frequency/(sampling frequency/2), where the units of cutoff frequency and sampling frequency are the same (once a minute). And *n* is the order of the Butterworth filter. For a Butterworth low-pass filter, the cutoff frequency is the highest frequency that can pass through the filter, and signals with frequencies higher than the cutoff frequency are blocked by the filter. From the minute-level heart rate data for one day, a notable decrease in heart rate can be observed at the onset of sleep, and similarly, a notable increase can be observed during the waking phase. Therefore, the heart rate during the sleep phase is defined as the heart rate between the end point of the rapid decrease phase and the start point of the next rapid increase phase (the part between the two arrows in Figure S2). The daily average heart rate is the average of the sleep stages over the filtered heart rate.

Missing value processing

Heart rate data collected by the bracelet contained missing values, possibly due to participants not wearing the device on time. To ensure the accuracy of the daily average heart rate trend, we removed the parts of the data that were missing for more than 6 days within 30 days. Other missing values of no more than 6 days were supplemented using linear interpolation. In addition, we excluded data with less than 45 days of recorded data after removing missing segments, as a shorter data series could affect the accuracy of the filtered data. After processing for missing values, the resulting heart rate data included 47 ovulation records and 297 menstrual records.

DCT analysis

To confirm the existence of the monthly rhythm in the heart rate of fertile women, we analyzed the daily average heart rate data using The discrete cosine transform (DCT) spectral analysis.[37] The DCT analysis represents a finite sequence of data points by decomposing them into a sum of cosine functions with varying frequencies. We used DCT analysis to decompose the daily average heart rate into a series of cosine function coefficients with different frequencies using MATLAB software, where larger coefficients indicate a higher contribution of the corresponding frequency component in the input signal. For signals with periodicity, the frequency components tend to be concentrated at certain discrete frequencies, resulting in higher DCT coefficients at certain positions during the analysis. After applying DCT analysis to the daily average heart rate of women of reproductive age (Figure 1A), we found that the highest coefficient corresponded to a cycle length of approximately 30 days (the horizontal axis was converted from frequency to cycle length), indicating that the daily average heart rate of women of reproductive age exhibits a monthly rhythm.

To facilitate the observation of data periodicity in DCT analysis, it is essential to retain data with the longest possible duration when handling missing values. Therefore, the data selected for DCT analysis should have a minimum length of 60 days, ensuring that there are no more than 3 days of missing values within any 30-day interval.

Average daily heart rate smoothing

When searching for monthly rhythm features in the heart rate data, we used a Butterworth low-pass filter.[38] to smooth the data and avoid the influence of high-frequency noise (Figure S3A). To better reflect the rhythmic information in the heart rate, we chose a 6th order filter and a normalized cutoff frequency of 0.09. With this set of filter parameters, the filtered heart rate showed a notable monthly cycle.

Calcium signal data processing

In the study of activity and calcium signal in mice, the selected calcium signals were measured under dark conditions, after two weeks of 12 h:12 h dark-light alternation.[20,21] To discover the characteristics of the offset of mice activity on the calcium signal, we first smoothed the data. The calcium signal was filtered using a 2nd order Butterworth low-pass filter with a normalized cutoff frequency of 5×10^{-5} by MATLAB software. Further, we calculated the derivative curves of the filtered calcium signals, which are the velocity trajectory profiles, and averaged the velocity trajectories of the calcium signal for four mice. On the other hand, from the actogram of mice wheel running, we observed the average time of the mice activity offset, which was strongly associated with the maximum value of the velocity trajectory of the calcium signal.

QUANTIFICATION AND STATISTICAL ANALYSIS

All the statistical analyses were performed using spearman correlation analysis with the software Matlab 2019b. The $p < 0.1$ was considered statistically significant.